Precise state-of-charge mapping via deep learning on ultrasonic transmission signals for lithium-ion batteries

Zhenyu Huang[a,b], Yu Zhou[b], Zhe Deng[b], Kai Huang[a], Mingkang Xu[b], Yue Shen[a], and Yunhui Huang[a*].*

[a] State Key Laboratory of Material Processing and Die & Mould Technology, School of Materials Science and Engineering, Huazhong University of Science and Technology, Wuhan, Hubei, People's Republic of China

[b] Wuxi Topsound Technology Co., Ltd., Wuxi, Jiangsu, People's Republic of China

[*]Corresponding authors.

Email address: shenyue1213@hust.edu.cn; and huangyh@hust.edu.cn

Name	Model	Parameter
Mechanical module	NSS75-L10-S300-S450	Move precision 0.02 mm
Ultrasonic T&R circuit	Ultra Jet	25~400 V, 0.3~10 MHz
Ultrasonic transducer	1.0C14F40	1.0 MHz, Beam diameter(-6dB) 2.0mm
Data acquisition card	ATS9350	10~250M Samples/Second
Temperature-controlled bath	BH8104	-20~80 ℃，±0.5 ℃
Silicone oil	Polydimethylsiloxane	10cSt

Table S1 The ultrasonic battery scanning system components version and parameters

Cathode		Anode	
Ingredient	Ratio (wt %)	Ingredient	Ratio (wt %)
LCO	96.1%	AG	95.3%
Super-P	1.6%	CMC	1.3%

		(Carboxymethyl Cellulose)	
CNT (Carbon nanotubes)	0.6%	SBR (Polymerized Styrene Butadiene Rubber)	2.2%
PVDF (Polyvinylidene difluoride)	1.7%	Super-P	1.2%

Table S2 Cell structure details

Testing procedure and data collection:

In this work, the data collection of cells (Cell #1-6) mentioned in this work were both measured by TOPS-LD50A ultrasonic battery scanning system, and cells were scanned column by column in a snake manner under different SoCs as indicated in **Fig. S1**. The scanning range of cells was both 45*75 mm, and the raw acoustic data was collected and saved as a 45*75 matrix simultaneously. Each element in the matrix is a 10000-length vector, i.e., $[\boldsymbol{\alpha_1}, \boldsymbol{\alpha_2}, ..., \boldsymbol{\alpha_{10000}}]$, it also corresponds to the transmitted ultrasonic signal of 1 mm * 1 mm area on cell.

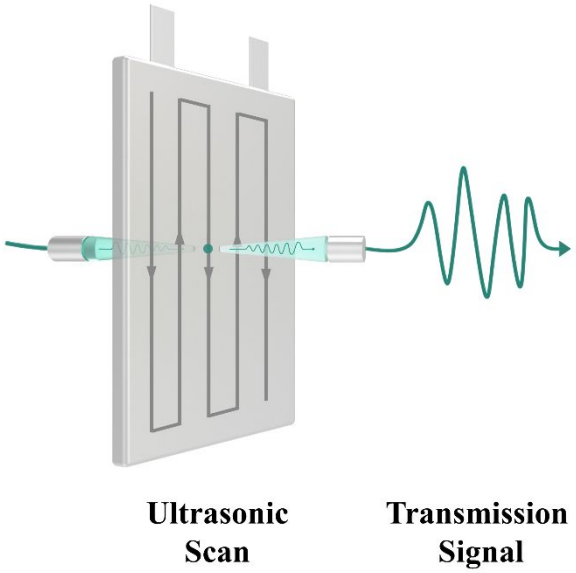

Fig. S1 Diagram of the ultrasonic testing procedure.

Electrochemistry cycling		Protocol
Charge process	Segment 1-19	Constant current 0.3 C, 1/6 h
		Rest 25 minutes
	Segment 20	Constant current 0.3 C, Constant voltage 4.25 V, terminal current 0.05C
		Rest 25 minutes
Discharge process	Segment 1-20	Constant current 0.3 C, 1/6 h
		Rest 25 minutes

Table S3 Cycling protocol

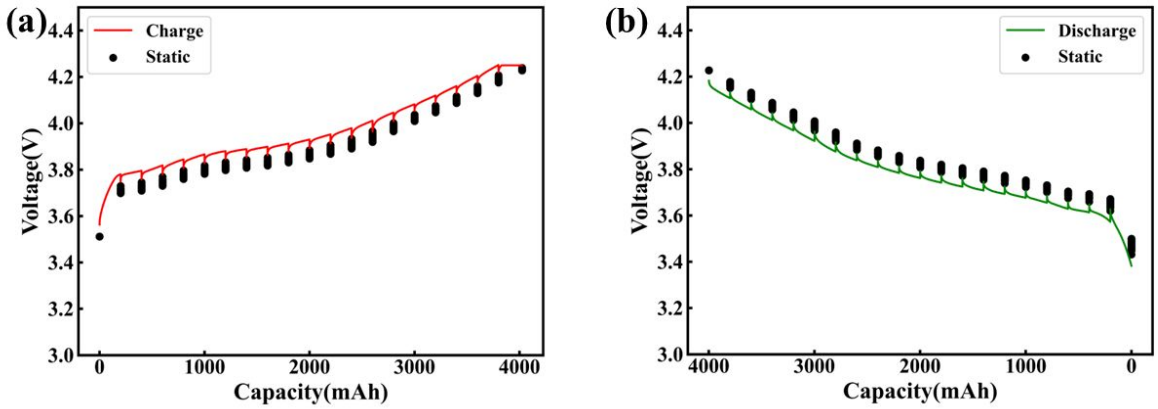

Fig. S2 Electrical experimental data. (a) and (b) are voltage versus capacity curve during charge and discharge, respectively.

Data for acoustic response to SoC changing:

The raw scanning acoustic matrix data of Cell #1-3 under different SoCs were collected by using the testing method mentioned above. Then, these data were used to analyze the acoustic response to SoC changing, the results were shown in the manuscript Fig. 1.

In Fig. 1 a-d, these transmitted ultrasonic waveforms at a certain position were chosen from the raw scanning acoustic matrix data of Cell #1 at different SoCs, which were measured by the method mentioned above.

In Fig. 1 e-g, the spots of different colors represent the characteristics of the transmitted ultrasonic signal of different positions on different cells, these positions were randomly selected,

and the ultrasonic signals were chosen from the raw scanning acoustic matrix data of Cell #1-3 under different SoCs to further obtain the characteristics of each signal.

Variance filtering:

By using the ultrasonic battery scanning system, the acoustic data of different position on cell was collected point by point, and the single-point acoustic data format was saved as:

$$\boldsymbol{A_I} = [\boldsymbol{\alpha_{i,1}}, \boldsymbol{\alpha_{i,2}}, \ldots, \boldsymbol{\alpha_{i,10000}}]$$

In order to reducing the computational complexity and shorten the model training time, we eliminate irrelevant features from these $\boldsymbol{A_I}$-like single-point acoustic data. Firstly, some single-point acoustic data were randomly chosen from the cell, and the collection of these data was shown as bellows:

$$\boldsymbol{B} = \begin{bmatrix} \boldsymbol{\alpha_{1,1}} & \boldsymbol{\alpha_{1,2}} & \cdots & \boldsymbol{\alpha_{1,J}} & \cdots & \boldsymbol{\alpha_{1,10000}} \\ \boldsymbol{\alpha_{2,1}} & & & & & \boldsymbol{\alpha_{2,10000}} \\ \vdots & & & & & \vdots \\ \boldsymbol{\alpha_{i,1}} & & & \ddots & & \boldsymbol{\alpha_{i,10000}} \\ \vdots & & & & & \vdots \\ \boldsymbol{\alpha_{\mathrm{n},1}} & \boldsymbol{\alpha_{n,2}} & \cdots & \boldsymbol{\alpha_{n,J}} & \cdots & \boldsymbol{\alpha_{n,10000}} \end{bmatrix}$$

Where n represents the amount of point that was chosen for variance filtering, J represents the data index of the single-point acoustic data. Each row data in B represents a single-point

acoustic data, and each column data (A_J) in $\boldsymbol{B}$ represents a collection of the value with the same index (J) in different single-point acousitc data ($\boldsymbol{A_I}$).

And then, we utilized the equation S1 to filtering irrelevant features from the the dataset $\boldsymbol{B}$.

$$\boldsymbol{Var_J} = \frac{\sum_{i=1}^{n}(\boldsymbol{\alpha_{i,J}} - \overline{\boldsymbol{A_J}})^2}{\boldsymbol{n-1}} \quad (1)$$

The variance filtering threshold was set to 0.001, which means the column data in $\boldsymbol{B}$ with the $\boldsymbol{Var_J}$ below threshold will be removed from the original data. Partial data with different general SoC was chosen to illustrate the principle of data dimensionality reduction in **Fig. S3**, in which these column data circled by red rectangle would be removed as a result of the variance is below the threshold.

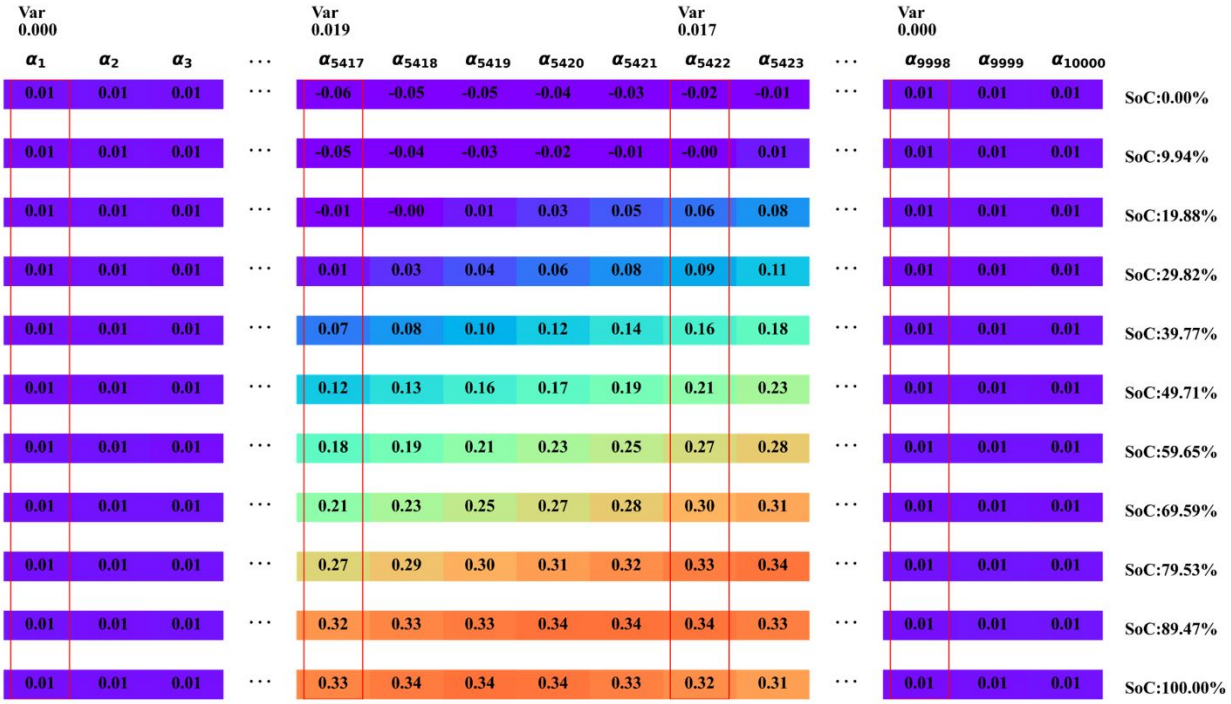

Fig. S3 Diagram of the acoustic data feature variance filtering.

Weights initialization:

The weight initialization approach is the truncated normal distribution (TND), and the probability density function (PDF) described as follows:

$$\boldsymbol{f(x;\mu,\delta,a,b)} = \frac{\frac{1}{\delta}\boldsymbol{\Phi}\left(\frac{x-\mu}{\delta}\right)}{\boldsymbol{\Phi}\left(\frac{b-\mu}{\delta}\right) - \boldsymbol{\Phi}\left(\frac{a-\mu}{\delta}\right)} \tag{2}$$

where x is one sample in X, and the distribution law of the sample in X obeys the condition: $X \sim N(\mu, \delta^2)$, $X \epsilon (a, b)$, $-\infty \leq a < b \leq \infty$. The left and right bounds of the truncated normal

distribution are a and b, and the sample mean and standard deviation are μ and δ. $\phi(\varepsilon)$ is standard normal distribution (SND):

$$\boldsymbol{\phi(\varepsilon) = \frac{1}{\sqrt{2\pi}} e^{-\frac{1}{2}\varepsilon^2}} \quad \textbf{(3)}$$

$\Phi(x)$ is cumulative distribution function (CDF):

$$\boldsymbol{\Phi(x) = \int_{-\infty}^{x} \frac{1}{\sqrt{2\pi}} e^{\frac{-t^2}{2}} dt} \quad (4)$$

We build a relatively good parameters for TND based on a thorough analysis of the data and parameter adjustments; **Fig. S4 b** illustrates the initial weight range.

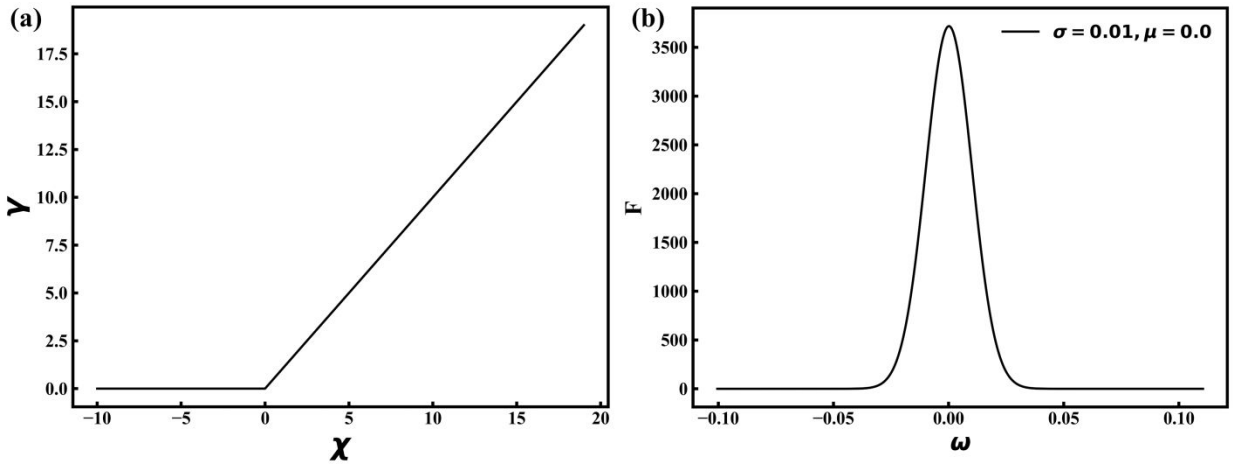

Fig. S4 Activation function and initial weight of FNN. (a) ReLU activation function, which represents the mapping from x to y; (b) PDF of TND, representing the range of $\boldsymbol{\omega}$ (the horizontal axis $\boldsymbol{\omega}$ represents the initial weight of FNN, and the vertical axis F represents the probability density).

Dynamically adjusting the learning rate:

The model callback function was setting to allow the dynamic adjusted learning rate, the parameter patience of the callback function was setting to 100, which means the learning rate would descend if the validation loss has no significant drop within 100 epochs, the parameter factor of the callback function was setting to 0.9, which means the learning rate would decrease by the factor of 0.9 each adjustment.

Regularization items:

Random dropout layers were added between the layers of the neural network, based on the analysis of training dataset size and the complexity of the neural network, we keep adjusting the random dropout ratio and evaluate performance on unknown cells, the random dropout ratio was finally set as 0.1, this means 10% of the neurons passing through this layer will be inactivated randomly, which can effectively prevent overfitting.

Data for FNN model training:

The raw scanning acoustic matrix data of Cell #5 under different SoCs were collected by using the testing method mentioned above. The training dataset was derived from the raw scanning acoustic matrix data of Cell #5 at 150 randomly chosen positions under 42 general SoCs. we also avoided the near tab areas for data selection and carried out the variance filtering method on these selected data.

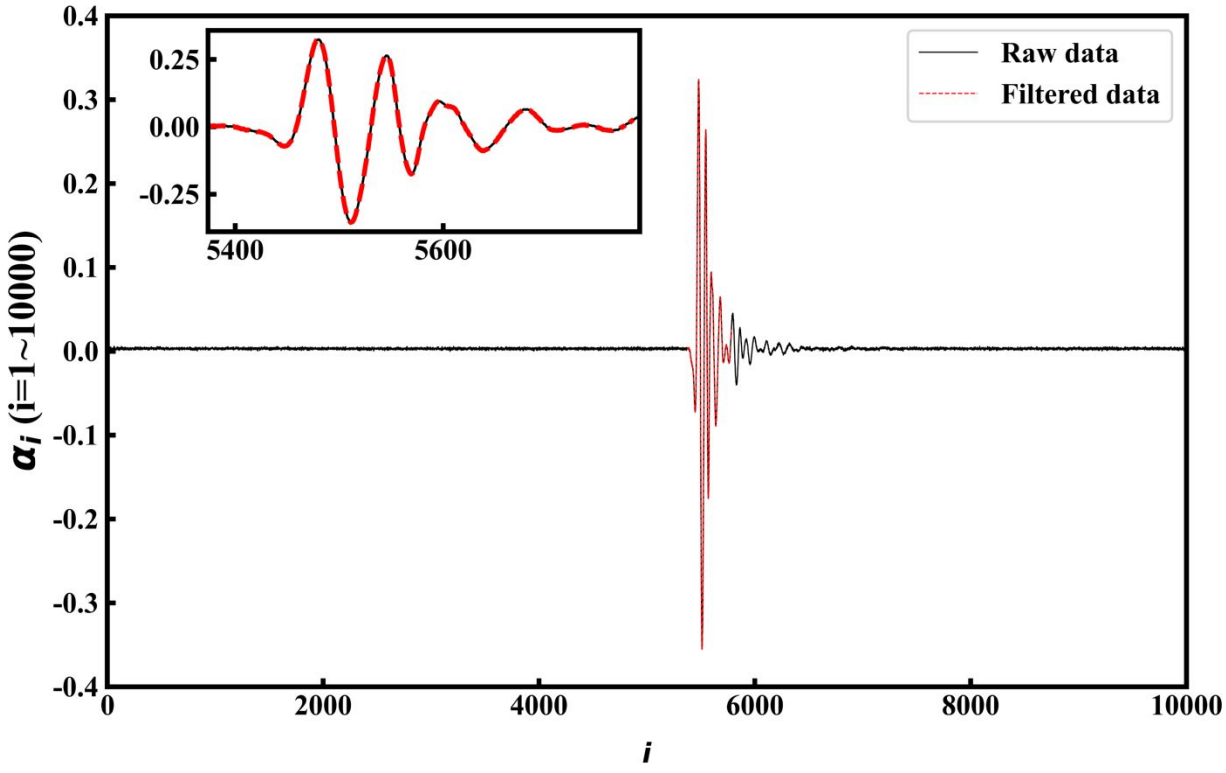

Fig. S5 The raw single-point acoustic data and the data after variance filtered;

Data for FNN estimated local SoC:

The raw scanning acoustic matrix data of Cell #4-6 under different SoCs were collected by using the testing method mentioned above. Cells (Cell #4-6) were disassembled and the anodes were punched with a 6 mm puncher at 6 different positions as indicated in Fig. 3. The FNN estimated SoC at these positions were obtained by inputting the ultrasonic signals located in these positions to the well trained FNN model, while these ultrasonic signals were extract from the raw acoustic matrix data by positional information.

ICP-OES samples preparation and characterization:

As shown in Fig. S6, 18 samples are cut off from the same 6 positions on 3 pieces anode layers in the Ar atmosphere glove box, which were used to characterize the amount of the inserting lithium. Three cells were charged to 30%, 50%, and 70% SoC, then disassembled in a glove box, the double- coated anodes are obtained. By using hole puncher (MSK-T10) on the anode, a circular sample with a diameter of 6mm can obtain. Rinse these samples with dimethyl carbonate (DMC) for 10 minutes, and then spry in a vacuum dryer. The amount of lithium in samples is characterize by the inductively coupled plasma (ICP-OES: Thermo Fisher iCAP PRO, RF power: 1150W, Plasma flow: 0.5L/min, Auxiliary flow: 0.5L/min, Nebulizer flow: 125.5L/min, Simple uptake delay: 30s). The sample was dissolved with acid and then 1-fold diluted for measurement.

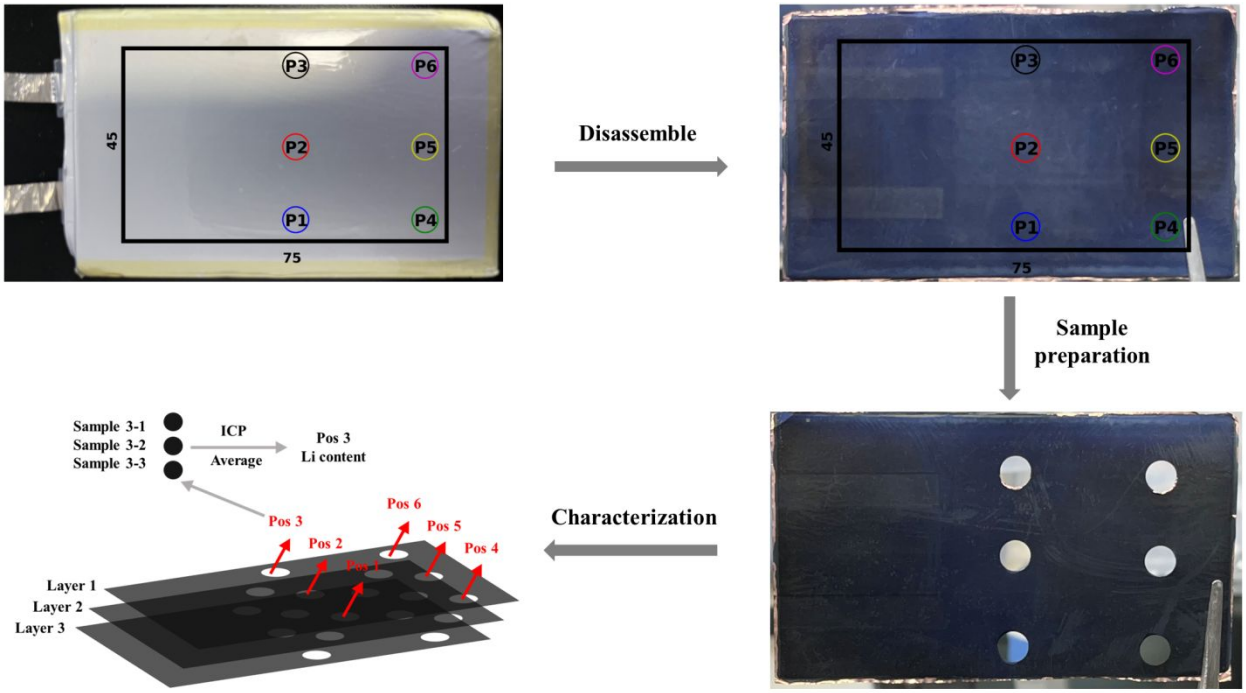

Fig. S6 Sample preparation and the measurements of lithium content in sample.

ICP-OES measured SoC calculation:

The lithium content in anode samples were determined by solution analysis with ICP-OES, and the ICP-OES measured SoC of each sample can be calculated by bringing the lithium content into the equation as follows:

$$SoC = \frac{\frac{m}{Mr}}{\frac{c}{Fx}\frac{\pi r^2}{abl}} = \frac{xmFabl}{cMr\pi r^2} \quad (5)$$

where the Mr (= 6.94g mol^{-1}) is the molar mass of the Li, the F (=26.8 Ah) present the capacity bring by 1 mole electrons in the Li_xCoO_2/Graphite system battery, the r is the radius of the sample,

the a is the width of the anode, the b is the length of the anode, the l is the number of anodes, the c is the specified capacity, these parameters value are shown in **Table S4**. When the cell was charging from 3.3 to 4.25 V, Li_xCoO_2 could be assumed to delithiate in the range x = 0.95 to x = 0.5 from top of charge to bottom of charge[1-3].

Parameter	Value
Li molar mass (Mr)	6.94 (g/mol)
Capacity of 1mol electronic (F)	26.8 (Ah)
Molar coefficient (x)	0.45
Radius of sample (r)	3 (mm)
Anode width (a)	57 (mm)
Anode length (b)	92 (mm)
Anode layers (l)	18
Battery capacity (c)	4 (Ah)

Table S4 ICP-OES measured SoC calculation parameter value

Iterative adjustment process data:

In this work, we have made many efforts to optimize the dataset collection, neural network structure, and hyperparameters, the compare of FNN estimated SoC and ICP-OES measured SoC

during the whole iterative adjustment process was shown in Fig S7. The meaning of M1, M2, and M3 were list as follows:

M1: data variance filtering, and weights initialization. Meanwhile, we avoid chosen the data from the near tab areas to reduce the impact of these data on the FNN model. Combine with these two methods, the model training time was shortened, the convergence rate was speed up, the performance of the FNN model was promoted, the RMSE of the FNN estimated SoC was reduced from 23.22 (raw acoustic data and initial FNN model) to 12.14.

M2: dynamically adjusting the learning rate. This method increases the FNN model iteration period, which helps to improve the SoC estimated accuracy of the model. Finally, the SoC estimated accuracy of the model on the source cell from which the training dataset is chosen is significantly improved. Additionally, the RMSE of the FNN estimated SoC was reduced from 12.14 (M1) to 11.01.

M3: regularization items. Based on the previous work and results, we further added regularization terms to the model, which would increase the random dropout ratio to prevent overfitting, and the SoC estimation accuracy on different cells were improved, the RMSE of the FNN estimated SoC was reduced from 11.01 (M2) to 3.02.

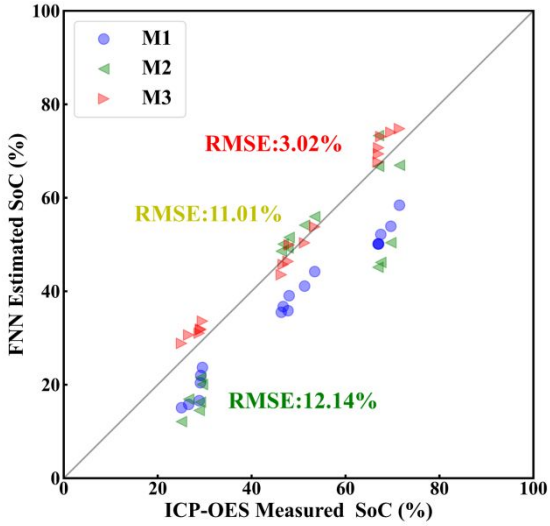

Fig. S7 Comparison of the FNN estimated local SoC and ICP-OES measured local SoC value during the iterative adjustment process.

Data for SoC mapping of cell:

The raw scanning acoustic matrix data of Cell #4 under different SoCs were collected by using the testing method mentioned above. The ultrasonic signal on each position was successively chosen from the raw scanning acoustic matrix data (dimension: 45*75) of Cell #4 under different SoCs, the FNN estimated SoC on each position was obtained by inputting the ultrasonic signal to the trained FNN model. Then, these FNN estimated SoCs of Cell #4 during charge were presented in the form of SoC mapping as indicated in Fig. 4 a.

REFERENCES

1. Amatucci, G. G.; Tarascon, J. M.; Klein, L. C. CoO_2, The End Member of the Li_xCoO_2 Solid Solution. *J. Electrochem. Soc.* **1996**, *143* (3), 1114-1123.

2. Reimers, J. N.; Dahn, J. R. Electrochemical and In Situ X-Ray Diffraction Studies of Lithium Intercalation in Li_xCoO_2. *J. Electrochem. Soc.* **1992**, *139* (8), 2091-2097.

3. Dahn, J. R. Phase diagram of Li_xC_6. *Phys. Rev. B* **1991**, *44* (17), 9170-9177.